

CHAPTER 2:
TWO-BEAM-COUPPLING MODULES

2.1. INTRODUCTION

The development of photorefractive processing systems, consisting of two or more photorefractive elements, is stymied by the lack of a well-developed component technology which would allow for rapid proof-of-concepts and testing of systems without the burden of extensive, time-consuming element-by-element alignment, as is the case of conventional photorefractive systems.

As a first step towards the development of photorefractive component technology, we developed modular photorefractive units that could be easily interconnected by the use of multimode, optical fibers. The main idea is to have the photorefractive crystal within a module and its associated fiber optic elements optimized for a specific photorefractive function and then permanently fixed in place. The modules are connectorized, and may be interconnected with multimode fibers in any desired configuration. Thus, the assembly of a complete optical system never entails alignment of beams through crystals or other optical elements which are part of each photorefractive function. This means that, with a collection of appropriate modules in hand, a complex system can be quickly assembled or reconfigured.

The geometry of each module can be optimized to perform any of the common wave-mixing effects that have found their way into conceptual and real processing systems, such as two-beam coupling gain [Khuktarev,'79], novelty filtering [Anderson,'89;Horowitz,'91a], four-wave mixing [Cronin-Golomb,'84;Feinberg,'83], self- and mutually-pumped phase conjugation [Feinberg,'82;Sharp,'94;Yeh,'92], photorefractive oscillation [Anderson,'92;White,'82;Yeh,'85], and more. Because it is employed ubiquitously in the photorefractive systems developed in our laboratory, two-beam coupling is the function of choice to test the modular concept.

To this end we have built several two-beam coupling photorefractive modules, such as the one shown in figure 2.1. This chapter discusses the development of these two-beam coupling modules, starting with design considerations, followed by the alignment procedure and the resulting characterization parameters. In the last section of the chapter we test the performance of the modules when these are interconnected to form a photorefractive system, namely an auto-tuning filter, the functioning of which is explained in that section.

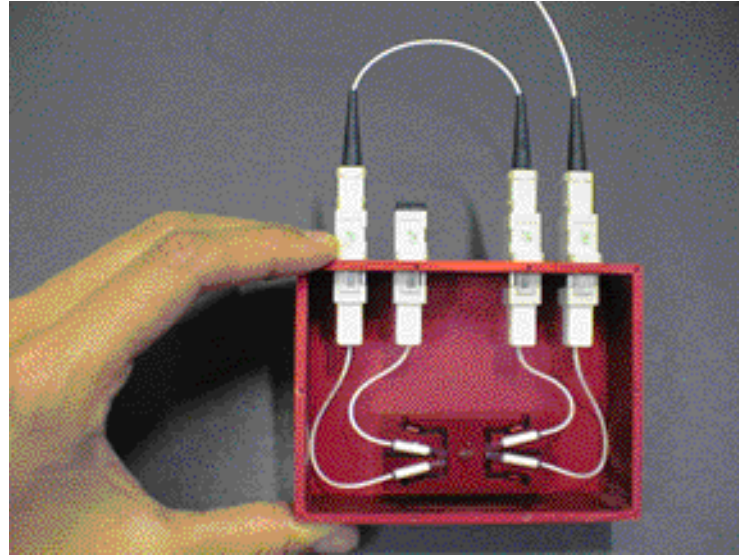


Figure 2.1. Two-beam coupling module. The picture shows a ring oscillator which is obtained by simply using an optical fiber to connect the output signal port (gain port) to the input signal port. Another fiber provides the input pump.

2.2. THE MULTIMODE FIBER OPTICS INTERCONNECTIONS

A basic step in designing a component technology for photorefractive systems is determining the kind of interconnections that should be used. The choice is basically between using free-space optics or fiber optics. Multimode fiber optics was selected because, as mentioned above, the use of connectorized fibers dispenses with the need for alignment between modules, therefore offering enormous benefit of ease of assembly and reconfiguration. In addition, the fiber-interconnected modules derive benefits from the substantially well-developed multimode fiber component technology, which provides us with standardized connectors and a gamut of fiber

terminated optical devices. What are the tradeoffs of such benefits? This brief section clarifies the way in which the use of multimode fibers affects the modules.

One major drawback of multimode fibers as opposed to free-space, Gaussian beams is that two-beam coupling gain is reduced, partly because of the nature of speckled beams [Zel'dovich,'95] and partly because of polarization scrambling by the fiber. The electro-optic coefficients in barium titanate are such that the ordinary component of the incident light polarization experiences a negligible two-beam coupling gain, and in addition, it partially erases the grating associated with the extraordinary component. This causes a reduction of the modulation index and, therefore, the gain. Polarization effects can be mitigated by adding small polarizers to the modules, but in our modules we simply accept the sacrifice in gain for the sake of simplicity.

Multimode fibers were used as opposed to single mode, not only because it is much easier to couple a beam into it as compared with the latter, but most importantly, because a multiplicity of modes are necessary for image processing applications, and other photorefractive signal processing applications as well, such as the autotuning filter described in the end of this chapter. A common misconception regarding the multimode fiber optics interconnections is that its use excludes the modules from image processing applications. This is not generally the case. The multimode optical fiber interconnections permit one to process two-dimensional spatial information. Naturally, two-dimensional data becomes scrambled as it propagates down the fiber, however the information contained in the data is preserved provided there are no severely mode-dependent losses. Many image-processing tasks

and algorithms, such as sorting or pattern recognition, are indifferent to scrambling, i.e., the presence of an unscrambled version of the processed image in the output of a system is not essential to its function. Nevertheless, if the unscrambled output image is desired, one can recover such image by holographically correlating the speckle-field output, the scrambled output image, of a fiber-based system with the unscrambled input images. Even if the application is intolerant of scrambling, the fiber-interconnected modular approach may still allow one to explore processing concepts en route to the design of a specialized optical circuit.

Our graded-index fiber interconnections have a 62.5 μm core diameter and 125 μm cladding diameter. If its numerical aperture of about 0.26 is filled, the fiber will contain on the order of 16,000 modes if illuminated with a 514 nm laser.

2.3. DESIGNS AND RESULTS

As shown in figure 2.1, a two-beam coupling module consists of a barium titanate crystal located in the center of a monolithic aluminum base, and in between two pairs of collets, one input and one output pair. An interbeam angle of about 15° is theoretically calculated to provide maximum gain for barium titanate, however, given the collet's diameter of 3 mm, the interbeam angle between the two collets in a pair is chosen to be 30° as a trade-off to reduce the module's length to about 50 mm. Each collet lies on an independent flexured platform which can be tilted to compensate for small fabrication errors in the parts. This tilt is adjusted by set screws accessible from

the bottom of the base (see figure 2.2). We have tested several base versions with different designs for the flexures and corresponding tilt adjustments.

A top and side view schematic of a module is given in figure 2.2. Two laser beams enter the unit via optical fibers, are collimated by the lenses in the input collets, and then cross in the crystal where they undergo photorefractive two-beam coupling. After traversing the crystal, the loss and gain beams are collected by lenses in the two output collets and focused into another pair of optical fibers. The input and output fibers are terminated with connectors, and the base, along with the connectorized fibers, are assembled in a box, (as shown in figure 2.1).

This design of the modular units optimizes the photorefractive crystal geometry. Small beam diameters between $100\ \mu\text{m}$ to $820\ \mu\text{m}$ allow for small crystals and an efficient use of crystal volume: the length of the crystals typically varies between 2.5 and 4 mm, the cross-section is about $(1.5\ \text{mm})^2$. We get roughly 8 module crystals from a typical $(5\ \text{mm})^3$ barium titanate piece with the appropriate c-axis direction.

We have tested several modules with different combination of base designs, lenses and crystal cuts. Below we discuss the original design followed by our improved, latest design.

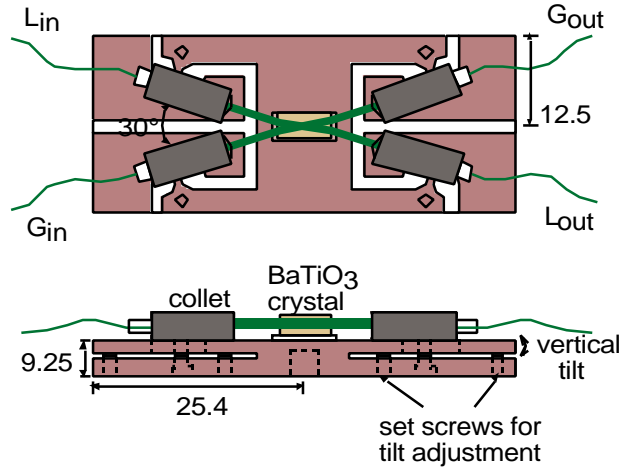


Figure 2.2. Schematic with top and side view of two-beam coupling module. A BaTiO₃ crystal is placed at the center of the unit over a small glass mount. Collets lie on platforms whose vertical tilt can be adjusted by two set screws. Dimensions are in millimeters.

2.3.1. The original design

The original modules contain the collet design described below and rectangular crystals.

A cross-section of a collet is shown in figure 2.3. The collets contain a 2mm-focal-length aspheric lens (350150 GeITech) which is glued to the collet with UV curing optical adhesive. A 62.5 μm core diameter fiber is inserted into a ferrule, attached with epoxy, and its end polished flush with the ferrule's face to provide an optical quality surface. The prepared ferrule is then inserted into the collet and a specially designed tool, which moves the collet-lens assembly with respect to the

ferrule, is used to collimate a 514 nm laser beam exiting the lens. The two pieces are then fixed with epoxy. The resulting beam diameter is approximately 820 μm .

The crystals were rectangular with a 20° or 30° cut with respect to the crystal axis. Maximum gain is typically achieved for a 45° cut, however the benefit of such gain maximum is associated with unwanted fanning. [Zozulya, A.,'95] Fanning reduces the dynamic range of the two-beam-coupling module, but the effect can be ameliorated by simply reducing the crystal-cut angle, which reduces the gain. The crystal-cut must be tailored to the application at hand. For the applications in our laboratories, high gain is typically desired so the 30° -cut crystals were more successful. All crystals were approximately $4 \times 2 \times 1.5 \text{ mm}^3$.

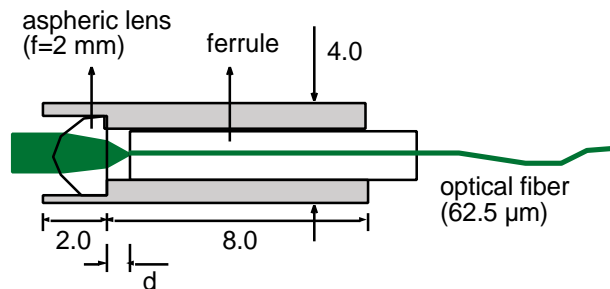


Figure 2.3. Cross-section of a collet with an aspheric lens (Geltech, 350150). The zirconia ferrule contains a polished multimode fiber with $62.5 \mu\text{m}$ core and $125 \mu\text{m}$ cladding. Distance d is adjusted to collimate the outgoing beam. All unspecified dimensions are in millimeters.

2.3.1.1. The alignment procedure

The alignment procedure, as depicted in figure 2.4, begins by mounting the module base on a rotation stage, and placing the crystal on a glass spacer at the center of the base. Next, each of two collets is attached to a jig. The jig consists of a two-dimensional translation stage with an extension arm with a beryllium-copper spring at the end, to which the collet is attached. The collets are positioned 30° apart at the input side of the base. They are made to completely contact the base by having the jig exert a light pressure upon them. With this arrangement a collet has four adjustment degrees of freedom: longitudinal and transversal translation, rotation about the axis through the center of the base and perpendicular to it, which we call “horizontal rotation”, and the “vertical tilt” provided by the flexured base. (The translation and horizontal rotation stage are shown in figure 2.4, whereas the vertical tilt, in figure 2.2).

Optimization of the photorefractive gain is the main goal in aligning the input collets. To do this 514nm Argon-Ion laser light is coupled into the input fibers and the overlap of the two beams inside the crystal is then maximized. This is accomplished by use of the longitudinal and transversal translation, and the vertical tilt. (Horizontal rotation is only needed when aligning the output collets.) Typically the gain is not uniform throughout the crystal’s volume. [MacCormack,'96] Therefore, one can search for a higher gain by simply moving the crystal sideways, so that the beam overlap probes different regions inside the crystal, and then select a particularly good position. To avoid problems when coupling into the output collets,

the beams must be parallel to the plane of the base. Once the optimal gain is obtained, the crystal and input collets are fixed to the base with epoxy and the jigs are removed.

The same pair of jigs are now used to position the two output collets to optimize the coupling of each beam into the respective output fiber. Finally, the two input and two output fibers are cleaved and terminated in SC connectors and the unit is enclosed in a $10.16 \times 7.62 \times 3.25 \text{ cm}^3$ box.

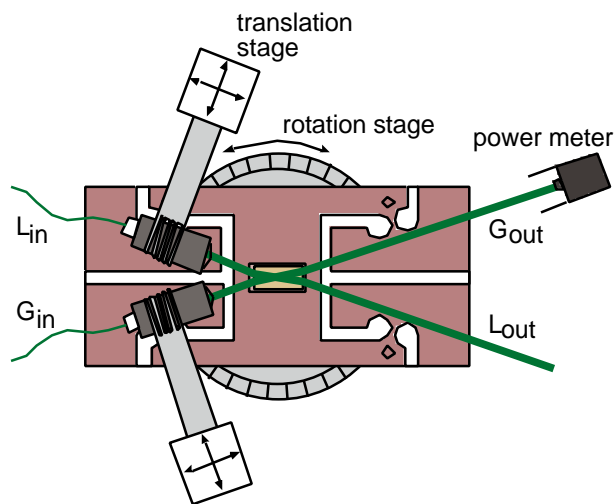


Figure 2.4. Setup for the alignment of the input collets. The gain is optimized by adjusting the translation stages and the set screws shown in figure 2. The rotational stage is used during the alignment of the output collets.

2.3.1.2. Results

Three quantities characterize these modules: gain, passive loss, and time response.

The gain is measured by taking the ratio of the output intensity of the gain-beam with the loss-beam unblocked over that with the loss-beam blocked. The gain measurements were obtained with an input intensity ratio of the loss-beam over the gain-beam of 3000. Three modules were built with 20°-cut crystals and they had gains of 12, 13 and 19, and another three were built with 30°-cut crystals having gains of 286, 406 and 435.

The passive losses are given by subtracting the passive signal coupling from one. The passive signal coupling was measured by taking the output to input intensity ratio of the gain beam while wiggling the fibers so as to impede the formation of photorefractive gratings in the crystal. The passive losses ranged from 72% to 84%, with an 80% average. We also measured a significant deterioration of the passive signal coupling due to alignment drift with a time scale of weeks. One of the modules passive losses went from 72% to 86% in about a month, whereas two other modules were completely misaligned after the same period.

To test the response time of the modules, we presented a step function to the input and measured the 10 to 90% rise time in the output. The input approximation to a step function, with a rise time of about 5 ms, was generated by manually unblocking the input gain beam. The measurements were performed with a loss beam power of 100 mW and a gain beam intensity of approximately 1% that of the loss beam. The output rise time was always between 500 and 700 ms.

2.3.2. The next generation

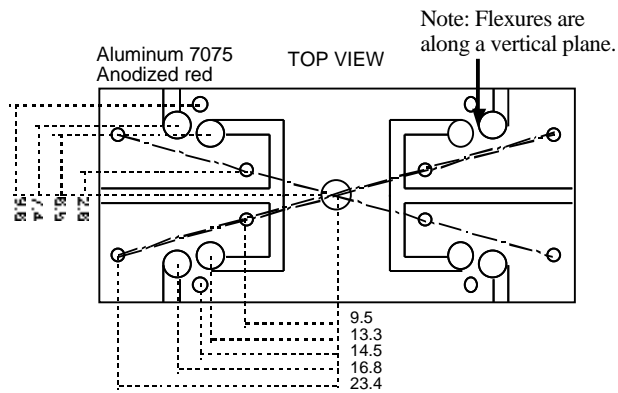
This section discusses, based on the above measured results, the routes for improving the module's design towards a new generation. Our primary concern is to reduce the passive losses and, most importantly, to improve the degradation with time of the passive signal coupling due to an alignment drift. Below we list the modifications made in the new design. The alignment procedure is similar to that of the first generation (section 2.3.1.1). The last subsection gives the results for the next-generation modules.

2.3.2.1. A new base design

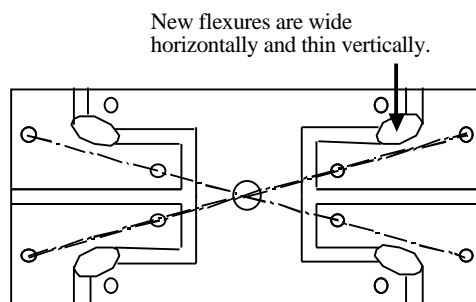
A top view schematic of the original base is shown in figure 2.5 (a). We call attention to the pivot points of the four flexured platforms. In this original base design, the pivots are wider vertically than horizontally (where horizontal is the plane parallel to the paper in the figure). We'll therefore designate these pivots as "vertical pivots". In some occasions the platforms pivots broke off during the modules' alignment procedure (see section 2.3.1.1 above). This happened because the height adjustment of the flexured platforms provided by these vertical pivots are insufficient for correcting nonidealities of the components in the modules. For instance, the crystal faces are not perfectly parallel, which cause the beams to be deflected. This suggests that the pivots could be significantly mechanically stressed even when they

didn't break. And most importantly, such stress is very likely the culprit for the alignment drift as the aluminum tries to relax.

To ameliorate the mechanical stress we tested several different base design modifications. The chosen design is the one shown in figure 2.5 (b), which is similar to the original, but instead of a vertical pivot it has a horizontal pivot (meaning that the pivot is wide in the horizontal plane and thin in the vertical plane). These allow for more range of height adjustment without sacrificing the tilt adjustment.



(a)



(b)

Figure 2.5. Details of the base design. Dimensions are in millimeters. (a) Original design with vertical pivots. (b) New base design is similar to the original, but with horizontal pivots which allows for greater

adjustment range. The ellipses represent milled slots resulting on wide but thin (about 750 μm) flexures.

2.3.2.2. Brewster-cut crystal

As explained in section 2.2 above, the ordinary (vertical) polarization partially erases the grating, reducing the gain. For two-beam coupling application, the greatest component of the unwanted vertical polarized light typically comes from the pump. So we designed a new “Brewster-cut” crystal geometry as shown in figure 2.6. The Brewster angle for barium titanate is 67° , and is obtained by neglecting the crystal’s anisotropy and using an refractive index of 2.4. Having the pump beam enter the crystal at Brewster’s angle increases the loss of the vertical polarization component to about 50%, while reducing the desired horizontal polarization component loss to less than 2%. The average reflection loss of the signal at 37° (such that angle of pump minus signal is 30°) is about the same as that at zero degrees, i.e. about 17%. Also, because the pump beam comes in at a steeper angle, it is wider inside the crystal than the signal beam: this facilitates alignment optimization for two-beam coupling. To reduce absorption losses, the new Brewster-cut crystals are 2.5 mm long, as opposed to the previous 4 mm length of the older rectangular crystals. The optical axis of the new crystals are oriented at 45° with respect to the input surfaces.

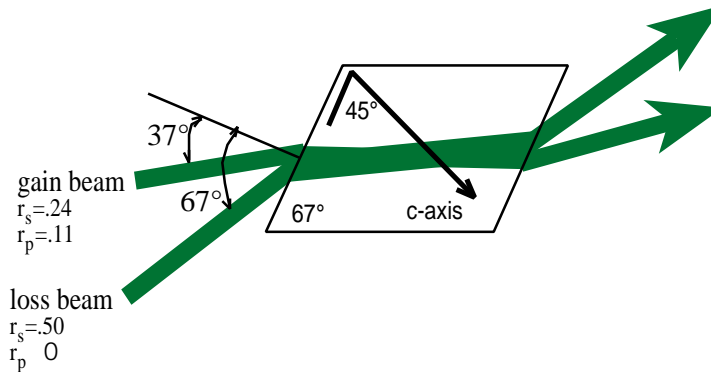


Figure 2.6. Top view of Brewster-cut crystal.

2.3.2.3. Graded-index lenses

Cheaper than the aspheric lenses, the graded-index (GRIN) lenses come in more variety, are easier to assemble, and dispense the use of collets or other mounts since they can be glued directly to the ferrule using optical adhesive for index matching. Figure 2.7 below shows a cross-section of the new ferrule-lens assembly. It is assembled by using a V-groove mount to align the center of the lens to that of the ferrule while curing the optical adhesive with UV light. The external end of the GRIN lenses were anti-reflection coated to reduce losses. We used a slightly focusing lens pitch (Selfoc SLW1.8 - .29 - 555 from NSG America) to decrease the beam diameter inside the crystal, resulting in beam diameters in the waist of about $100 \mu\text{m}$. The time response of a crystal is roughly inversely proportional to the total intensity of the beams. [Horowitz,'91b] This means that the smaller beam diameters should result in a decrease in the response time of the modules.

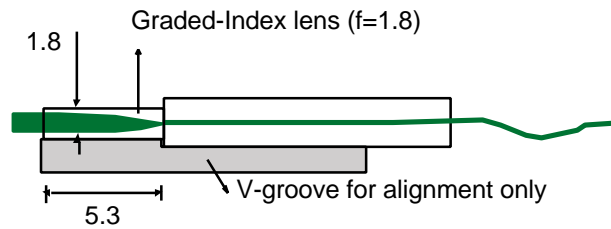


Figure 2.7. Cross section of new lens-ferrule assembly. A schematic of the v-groove is shown but it is removed after alignment. The fiber output will be imaged by the lens at a distance of about 6.3 mm from the output surface of the lens.

2.3.2.4. Buffered fibers

The optical fibers used in the first-generation modules were fibers having only a 245 μm diameter coating over its 125 μm diameter cladding (62.5 μm core). The operation of the modules is sensitive to acoustic vibrations, which disturb the fibers, change the speckle configuration, and thereby affect the two-beam coupling grating. When the modules are tested in a ring configuration such vibrations cause the so called “breathing” in the output, meaning that the output would slowly turn on and off. To ameliorate this effect, we switched to fibers having a 900 μm buffer jacket which helps isolate them from external vibrations. The buffered fiber also has the advantage of greater mechanical resistance, are white, and therefore are easy to see in a darkened room. Not only did we use these buffered fibers in some of our new

modules, but also, and perhaps most importantly, we used them in all the new module-to-module fiber cables.

2.3.2.5. Results for the new generation

We built a total of 3 modules with the above modifications. These modules are characterized in a similar way as described for the earlier modules (see section 2.3.1.2). The resulting small-signal gains are 526, 664 and 843; the passive losses are 68%, 73% and 72%; and the 10 to 90% rise time at the output when the input is unblocked is 120, 164 and 122 msec, respectively.

The higher gain is most likely due to a combination of factors. First, the Brewster-cut crystal geometry, which, as discussed earlier, increases the gain by reducing the ordinary polarization component. Second, the gain characteristics of the particular boule from which the crystals were cut. We have very little control over the material properties of the crystals, making it hard to discern how much each of these two effects contributed to increasing the gain.

The passive-loss average of 71% is about 10% less (better) than that of the first-generation modules. This number is due to a combination of loss components. We measured the absorption coefficient for barium titanate to be about 1.7/cm, resulting in a absorption loss of 35% for a 2.5 mm crystal. The reflection losses are approximately 25%: 50% reflection loss for the ordinary polarization and 0% for the

extraordinary polarization. The remaining 11% losses are consistent with typical measured coupling losses.

The alignment drift was, unfortunately, still present, however it was much less severe than in the first-generation modules. Two months after the above loss measurements were obtained, the measurements were redone and values had changed to 80%, 87%, and 79% respectively, corresponding to an average loss increase of 11%. The loss increase for all three modules is less than the loss increase for the earlier modules.

As expected, due to the smaller beam diameter, these modules responded an order of magnitude faster than the earlier ones. (Even though the pump beam diameter is increased by the Brewster incidence angle to about $250\ \mu\text{m}$, it is still smaller than the pump beam diameter inside the crystal in the first-generation modules of $850\ \mu\text{m} / \cos 15^\circ = 880\ \mu\text{m}$.)

2.4. DISCUSSION AND FUTURE DESIGN

The second-generation modules provided us with higher gain, lower losses and faster response time than the previous generation. However, an alignment drift is still present, though much less severe than before. This suggests that the components of the modules are performing well, but that the base is still mechanically relaxing causing the alignment drift. We believe the cause of this relaxation is due to the spring action of the flexured platforms. Such relaxation could be enhanced by either

temperature variations or shock. Therefore, as a future project for improving the modules we suggest that a new base be designed. Below we give some suggestions for a new base design, but before that, for the benefit of possible future designers, we first estimate the errors associated with the modules' components.

If further improvement of the base design is pursued, an assessment of errors and tolerances within the module will become necessary. The main misalignment causing errors are the following: the crystal's facet perpendicularity error, typically $\pm .015$ rad, the lens' facet perpendicularity error, $\pm .006$ rad, offset between the center of the lens and the ferrule, and lens tilt with respect to the ferrule. The offset between the center of the lens and the fiber is due to errors in the lens and ferrule radius ($\pm 5 \mu\text{m}$ for each), lens and ferrule nonconcentricity (negligible compared to diameter error), and the height error in the V-groove mounts used to align the lens to the ferrule (about $\pm 25 \mu\text{m}$). The total offset between the lens and ferrule in the object plane ($\pm (2.5^2+24^2) = \pm 25 \mu\text{m}$) is magnified 3.7 times by the lens resulting in a displacement of the beam in the image plane, which occurs inside the crystal, of $\pm 93 \mu\text{m}$. Given the distance of about 6 mm between the lens and the crystal, this displacement is equivalent to an angular error of approximately $\pm .015$ rad. Finally, one edge of the lens can be higher than the opposite edge (by $\pm 25 \mu\text{m}$), which will result in a lens tilt with respect to the ferrule (of $\pm .004$ rad for the 6 mm GRIN lens). This causes an angular deviation of the out-coming beam of $\pm .006$, calculated by using the GRIN lens ray-tracing matrix. Adding up all the contributions we get a total tilt error of $= (2.015^2+2.006^2)= .023$ rad. The current optical length between the

coupling lenses in the module is about 10 mm, resulting in a displacement error of 230 μm , as shown in figure 2.8.

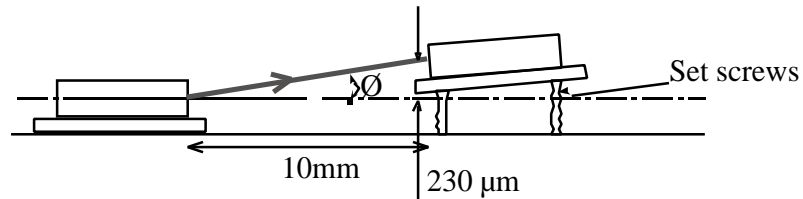


Figure 2.8. Representation of total displacement and tilt errors between lenses.

The main point in designing a new base is the following: Given that no adjustments are needed after the modules are ready, *all the adjustments should be external to the base design*. The base should serve solely to support the components, avoiding the use of internal adjustments (screws, springs, etc.), and thereby reducing the possibility of misalignment after the module is concluded. We suggest a design for the base where the crystal lies in the center of the base, shown in figure 2.9 (a). The five degrees of freedom for each collet would then be externally supplied by a “jig”, a 2-D tilt stage which is held by a 3-D translation stage. The main idea is to have the base with poles or blocks that slide up to almost meet the ferrules after they have been aligned. (A design with wide blocks is preferable to one with thin poles, as it is less susceptible to vibrations.) Low shrinkage epoxy is then used to fill the small gap between the ferrules and the base by capillary action. The ferrules should not move during the capillary process as they are held fixed by the jig. The epoxy used to

fix the ferrule to the sliding blocks and the sliding block to the base should have low shrinkage coefficient and low coefficient of linear thermal expansion (CTE). It should also have a low enough viscosity (< 1000 cps) so that it can wick into the gap between the ferrule and the pole or block. One viable epoxy is EPOTHIN from Bhueler with a shrinkage coefficient of .0002, CTE of $62 \cdot 10^{-6}/^{\circ}\text{C}$, and viscosity at 25°C of 200 cps. Another possibility is the EP30 from MasterBond with a shrinkage of .0003, which is slightly higher than that of the EPOTHIN but the CTE is lower, $35 \cdot 10^{-6}/^{\circ}\text{C}$, approaching that of aluminum, $24 \cdot 10^{-6}/^{\circ}\text{C}$, and of zirconia, $10.5 \cdot 10^{-6}/^{\circ}\text{C}$, the material used in the ferrules. One could also experiment machining the base out of a material with lower thermal expansion than the currently used aluminum. There are machinable ceramics whose CTE is close to that of the zirconia, such as AREMCO 502-400 with a CTE of $10.8 \cdot 10^{-6}/^{\circ}\text{C}$. The glass-ceramic material ZerodurTM is another possibility with CTE on the order of $10^{-7}/^{\circ}\text{C}$.

Besides a new base design, below are other possible modifications to take into consideration for a future design. Most of them involve a trade-off between gain and loss. One possible modification is to use rectangular cut crystals but with anti-reflection coatings on both input and output surfaces to reduce the reflection losses. However, that would allow both polarizations to enter the crystal and, as discussed earlier, would reduce the gain. That would also significantly increase the cost of the module. On the other hand, one could add polarizers to increase the gain. However, due to the speckle nature of the beams which scrambles the polarization, the polarizers would also increase the passive losses. Naturally, one more way to

manipulate the gain/loss trade-off is via the crystal's length, as more length implies more gain but also more absorption losses.

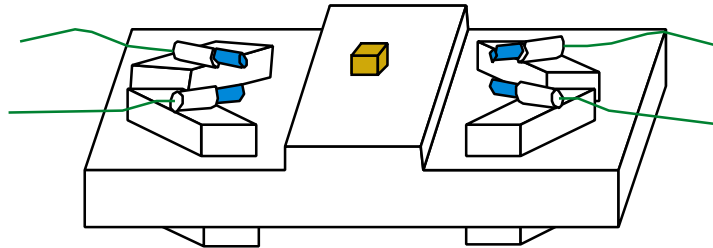


Figure 2.9. Suggestion for modular base design. Ferrule-lens assembly is adjusted externally by translational and rotational stages. Then the corresponding bases are slid upwards to meet the ferrule and glued with low shrinkage epoxy.

Finally, in a stretch of our imagination, it would be interesting if one could find a transparent liquid/gel substance which could solidify with extremely low shrinkage and without changing its refractive index. The ferrules could be positioned, with the use of pre-solidified bars of the same material, inside a mold containing the liquid material. The ferrules would then be aligned and the material in the mold solidified. Cut off the solidified bars that were originally holding the ferrules (which should now be sticking out), polish the six faces (assuming your mold was a parallelepiped) and you have it: a two-beam coupling module as a solid transparent piece (like the fossils in resin that you saw as a kid) with fibers sticking out.

2.5. AN APPLICATION EXAMPLE: THE AUTO-TUNING FILTER

Once the modules are in hand, building photorefractive circuits is trivial. The two-beam coupling modules can be quickly and easily interconnected to build and oscillator rings [Yeh,'85], reflexive-coupling units [Anderson,'95], and other systems. We tested the modules by using a ring oscillator with and without a reflexive coupling unit. This architecture is called the auto-tuning filter, an information processing system also known as the feature extractor [Zozulya, A. A.,'95], which we describe in this section as an example of the versatility provided by the modules.

Given two or more temporally and spatially orthogonal signals superimposed on a common input beam, an auto-tuning filter is a self-organizing system that learns to select the strongest input signal from within all the other input signals, in other words, it performs a principal component extraction. It consists of a photorefractive ring resonator with a common input beam as the pump. The non-linear dynamics in the crystal causes a competition of the signals for the resonator modes; the signal with the greater optical energy wins. For simplicity, only two input signals are used in our experiment. We built the auto-tuning filter system in the two different configurations shown in figure 2.10: as a simple ring oscillator and as a ring oscillator with a reflexive-coupling unit inside the ring.

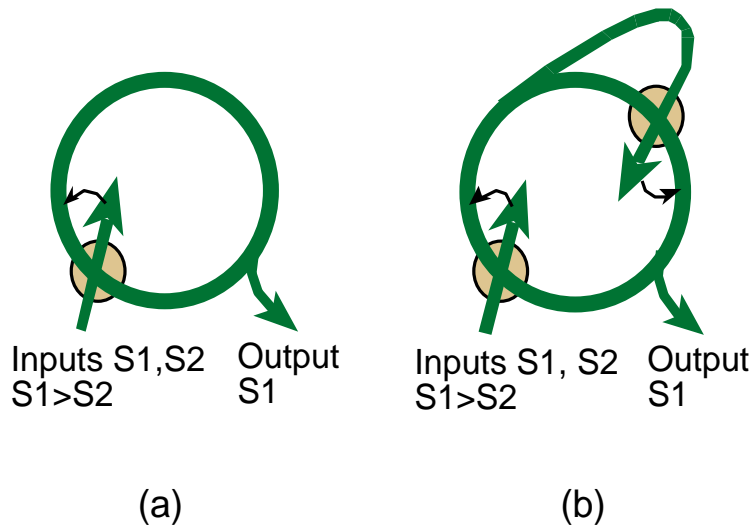


Figure 2.10. Autotuning filter in two different architectures: (a) simple ring, and (b) ring with reflexive coupling. The photorefractive crystals are represented by the circles.

Reflexive coupling [Anderson,'95] increases the competition between the signals that oscillate inside the ring, enhancing the selectivity of the auto-tuning filter. In simplified terms, the reflexive-coupling works as follow: A fixed fraction of these oscillating signals is split away from the ring and folds back to cross the ring inside the reflexive-coupling crystal. Part of these split signals are then coupled back into the ring - the strength of this coupling is dictated by the strength of the photorefractive grating written by each signal. These two signals compete for the available gain in the crystal. The weaker signal writes a weaker grating and thus experiences greater round-trip loss, which results in an even weaker signal, and so on, while the stronger signal undergoes the opposite behavior. Ideally, this positive feedback process continues until the weaker signal is totally inhibited by the stronger

one. In practice though, total inhibition of the weak signal is defeated by fanning [Zozulya, A.,'95] of the loss beam into the ring.

Figure 2.11 shows the experimental setup for the auto-tuning filter with reflexive-coupling. The laser beam is split by a polarized beam splitter; the intensity ratio of these two input beams is adjusted by the half-wave plate preceding the beam splitter. Each beam goes through an acousto-optic modulator (AOM) with 60% diffraction efficiency in the first order. The AOMs perform two functions: they shift the optical carrier frequency, resulting in a frequency separation of 280 MHz between the two input beams, which guarantees their temporal orthogonality; and they act as shutters to time modulate the optical carriers with the two input signals, single-sided square pulses at 1 kHz and 625 Hz respectively. The duty cycle of these pulses is set at 90% for low power loss. The two signal beams are then coupled into optical fibers and mixed by a directional coupler. To have the same contribution of each signal in the mixed input, a .50/.50 directional coupler is used (meaning that half of each incoming signal beam is coupled to each outgoing fiber). The beam of one of these outgoing fibers is directed to a photodiode, and the other is photorefractively coupled into the resonating modes of the ring by the pump unit, forming the oscillating beam. A second directional coupler inside the ring splits the oscillating beam so that 90% is directed into the input loss port of the reflexive-coupling, and the other 10%, into the input gain port. Finally, a third directional coupler (.01/.99) is used to sample the ring, forming the output which is monitored by a second photodiode. The intensity of the two photodiode signals are displayed on a spectrum analyzer (HP 356A, 100kHz).

The experimental setup for the simple ring oscillator is similar to that of figure 2.11 except that reflexive coupling is bypassed with an optical fiber.

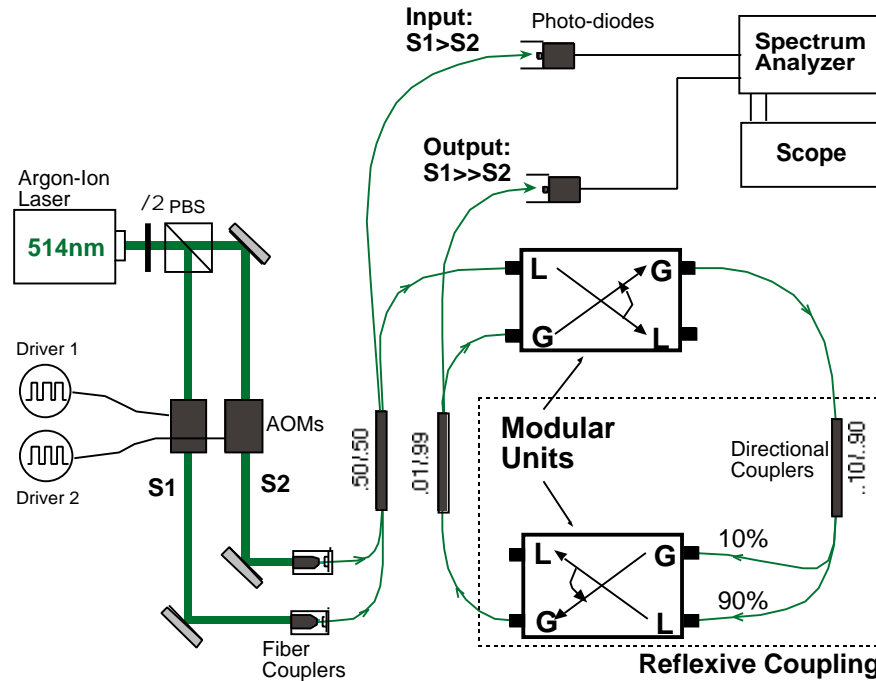


Figure 2.11. Experimental setup for the autotuning filter with reflexive coupling. The setup for the simple ring is obtained by simply bypassing the reflexive coupling. (PBS: polarized beam splitter, AOM: acousto-optic modulator.)

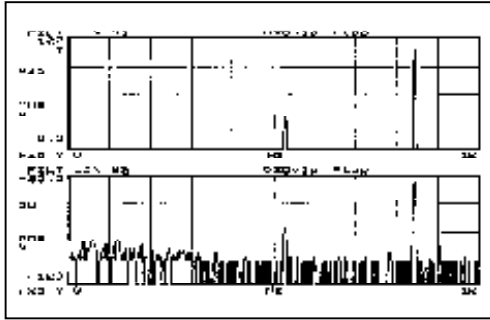
The effectiveness of the auto-tuning filter can be given by the contrast ratio (the strongest signal intensity over the weakest signal intensity) in the output, R_{out} , as compared to the contrast ratio in the input, R_{in} . Figure 2.12 shows the results obtained with an R_{in} of 3.17. The intensities of the input signals are shown at the top of the figures and that of the output signals, at the bottom. Figure 2.12 (a) shows the case of the ring with reflexive coupling. The resulting R_{out} is approximately 45 dB. We found

that the system could not self-start oscillation with R_{in} lower than 3.17. This is because the available gain in the medium is shared by the signals, meaning that the closer R_{in} is to one, the lower the gain available to the stronger signal. Eventually, when $R_{in} < 3.17$, this effective gain becomes lower than the minimum necessary for the system to self-start.

The effect of adding the reflexive coupling to the ring can be evaluated by comparing the result in figure 2.12 (a) with that in 2.12 (b). The absence of reflexive coupling in the simple ring configuration decreases the competition between the signals, resulting in a lower contrast at the output: R_{out} is about 38 dB, 7 dB lower than with reflection coupling. On the other hand, the removal of reflexive coupling also reduces the round-trip losses, which enables the system to self-start oscillation with lower R_{in} . The simple ring could self-start with R_{in} down to 1.75.

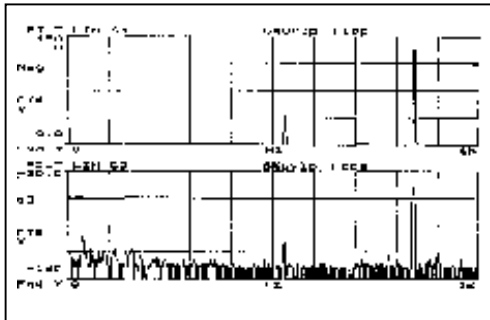
Finally, to check for asymmetries in the system, we switched the input signals of the ring with reflexive coupling, but keeping the ratio constant. The result is shown in figure 2.12 (c). R_{out} is 43 dB, 2 dB worse than the symmetric counterpart, corresponding to a 2:3 asymmetry. We believe this asymmetry is mostly due to the mode structure dependence of the directional couplers.

(a) Ring with Reflexive Coupling:



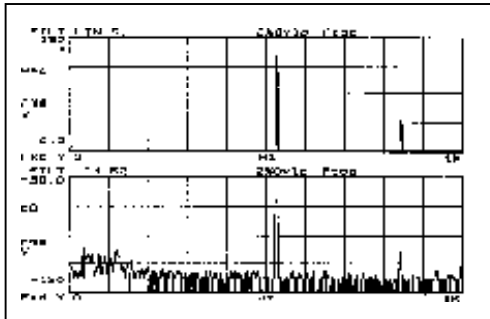
Input: $S1/S2= 3.17 \pm 0.1$
Output: $S1/S2= 45.4\text{dB} \pm 1\text{dB}$ (34 674)

(b) Simple Ring:



Input: $S1/S2= 3.17 \pm 0.1$
Output: $S1/S2= 38.2\text{dB} \pm 1\text{dB}$ (6607)

(c) Ring with Reflexive Coupling (symmetric case):



Input: $S1/S2= 3.17 \pm 0.1$
Output: $S1/S2= 42.5\text{dB} \pm 1\text{dB}$ (17783)

Figure 2.12. Input and output intensity spectra for the autotuning filter. Input spectrum is shown at the top of each screen with a ratio of 3.17:1 between the two input signals (linear scale); output spectrum is shown at the bottom (dB scale). (a) Ring with reflexive coupling, output ratio is 45 dB; (b) simple ring, output ratio is 38 dB; and (c) same as (a), except that the input signals are switched to check for asymmetries, output ratio is 43 dB. Reflexive coupling significantly enhances the selectivity.

2.6. CONCLUSIONS

On the auto-tuning filter application above, the use of the two-beam coupling modules allowed quick verification of the properties of the system, such as the fact that adding the reflexive-coupling increases the output contrast. In this context the modules have demonstrably fulfilled its purpose of supplying a means for quick testing of concepts and of new ideas in photorefractive systems. With a collection of different modules available, complex systems can be easily assembled and modified.

The specific modular design one chooses for a particular function, such as two-beam coupling, is always subject to improvements. In this chapter, we have shown the evolution from the original two-beam coupling modular design to an improved design rendering higher gain, lower losses and less long-term alignment drift. Suggestions for a future design to further reduce the drift is also given. Eliminating the long-term drift would add system reproducibility – after a modular system is disassembled it could be re-assembled exactly as before by simply using the same modules.

When building the modules one would want to tailor it to their applications. For example, the number of modules that can be cascaded, say, within a ring, is limited by the losses. Therefore, it might be of interest to further reduce the passive losses of each module, but keeping in mind the typical trade-off between gain and loss, as discussed at the end of section 2.4.